

Measurement and Control of Coulomb-Blockaded Parafermion Box

Kyrylo Snizhko,¹ Reinhold Egger,² and Yuval Gefen¹

¹*Department of Condensed Matter Physics, Weizmann Institute of Science, Rehovot, 76100 Israel*

²*Institut für Theoretische Physik, Heinrich-Heine-Universität, D-40225 Düsseldorf, Germany*

(Dated: April 12, 2017)

Parafermionic zero modes are fractional topologically protected quasiparticles expected to arise in various platforms. We show that Coulomb charging effects define a parafermion box with unique access options via fractional edge states and/or quantum anti-dots. Basic protocols for the detection, manipulation, and control of parafermionic quantum states are formulated. With those tools, one may directly observe the dimension of the zero-mode Hilbert space, prove the degeneracy of this space, and perform on-demand digital operations satisfying a parafermionic algebra.

Introduction.—Majorana zero modes are canonical examples for topologically protected quasiparticles with non-Abelian braiding statistics [1–4]. In the presence of Coulomb charging effects, intriguing features related to their non-locality have been pointed out [5–13] and probed experimentally [14, 15]. The drive for reaching universal quantum computation platforms and the quest to fully understand topological excitations have turned attention to exotic emergent quasiparticles such as parafermions (PFs) with $\mathbb{Z}_{n>2}$ symmetry. For PF zero modes, a plethora of interesting phenomena has been suggested in various platforms [16–28]; for a review, see Ref. [29]. For 1D interacting fermions, Majorana states are known to exhaust all stable possibilities [30], i.e., PFs can only exist under fine-tuned conditions [31]. However, for edge states of a fractionalized 2D system such as the fractional quantum Hall (FQH) liquid, domain walls between regions proximitized by a superconductor (SC) and a ferromagnet (FM) host stable PFs. Platforms for PFs include proximitized fractional topological insulators [16], bilayer FQH systems [25], and proximitized FQH liquids at filling factor $\nu = 2/3$ [22] or $\nu = 1/(2k + 1)$ with integer k [16, 18]. Such setups may ultimately provide a toolbox for generating Fibonacci anyons [22, 27], which, in turn, facilitate fault-tolerant universal quantum computation.

In the present Letter we leap beyond the interesting platforms alluded to above. We point out that PF devices dominated by Coulomb charging effects provide direct detection and manipulation tools targeting the fundamental physics of PFs. Specifically, we show below how one can (i) measure the dimension of the Hilbert space associated with PF zero modes, (ii) render this space degenerate in a controlled manner, and (iii) explicitly demonstrate the exotic algebra of PF operators. By combining systems made of fractionalized bulk matter with mesoscopic sensing concepts, all superimposed on Coulomb charging effects, the PF box (cf. Fig. 1) facilitates full access to the beautiful physics of PF zero modes without need for additional PF system hardware. Recent Majorana experiments [14, 15] also attest to the promise of such an approach. Probing these core facets

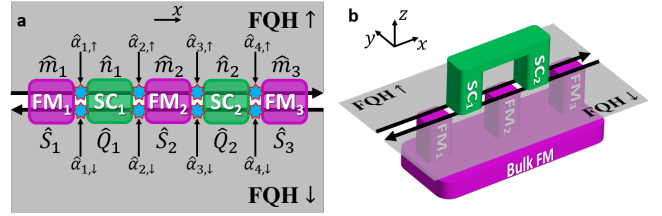


Figure 1. Schematic layout of the PF box. Panel (a) illustrates how two opposite-spin FQH edges (black arrows) are gapped out in distinct ways via proximitizing FM and SC segments in different regions. PF operators $\hat{\alpha}_{j,s}$ (blue stars) are localized at domain walls. Panel (b) indicates that SC segments are electrically connected to ensure phase coherence across different SC domains. Similarly, FM segments belong to one bulk FM.

of PF Hilbert space is realized employing fractional edge states [for current measurements] and quantum anti-dots (QADs) [for elastic cotunneling of quasiparticles through the box]. Such major facets are hard (if not impossible) to access otherwise, e.g., using multiple Josephson periodicities [16–18, 20, 21, 26, 32], zero-bias anomalies [23], split conductance peaks due to finite-size effects [24], or quantized conductance measurements [28, 32]. Apart from being interesting in its own right, e.g., in the context of topological Kondo effects [6], it stands to reason that the experimental implementation of the PF box would pave the way to realizing PF-based quantum information devices.

PF box model.—For concreteness, we study an array of PF zero modes implemented via two $\nu = 1/(2k + 1)$ FQH puddles of opposite spin [16, 18], cf. Fig. 1. With minor modifications, our concepts can be adapted to other platforms [33]. Moreover, for $\nu = 1$, PFs reduce to Majorana states and we recover the results of Ref. [12]. The puddle edges are described by bosonic fields $\hat{\phi}_{s=\uparrow/\downarrow=\pm 1}(x)$ with commutator $[\hat{\phi}_s(x), \hat{\phi}_s(x')] = i\pi \text{sgn}(x - x')$ and $[\hat{\phi}_\uparrow(x), \hat{\phi}_\downarrow(x')] = i\pi$ [18]. The resulting fractional helical edge state can be gapped by proximity coupling to SC or FM segments, see Fig. 1(a), with the Hamiltonian $H_0 = H_{\text{edge}} + H_{\text{SC}} + H_{\text{FM}} + H_{\text{C}}$, where $H_{\text{edge}} =$

$(v/4\pi) \sum_s \int_{-\infty}^{\infty} dx (\partial_x \hat{\phi}_s)^2$ with edge velocity v . Further,

$$H_{\text{SC}} = -\Delta \sum_{j=1}^N \int_{\text{SC}_j} dx \cos \left(\frac{\hat{\phi}_{\uparrow}(x) + \hat{\phi}_{\downarrow}(x)}{\sqrt{\nu}} + \hat{\varphi} \right), \quad (1)$$

$$H_{\text{FM}} = -t \sum_{j=1}^{N+1} \int_{\text{FM}_j} dx \cos \left(\frac{\hat{\phi}_{\uparrow}(x) - \hat{\phi}_{\downarrow}(x)}{\sqrt{\nu}} \right), \quad (2)$$

with the SC phase operator $\hat{\varphi}$ [39], and Δ (resp., t) being the absolute value of the induced amplitude for SC pairing (for tunneling between edge segments proximitized by FMs). All the proximitizing SCs (FMs) are implied to be parts of one common SC (FM), see Fig. 1(b). The SC is assumed to be floating (not grounded). With the SC charge \hat{Q}_0 , i.e., $[\hat{\varphi}, \hat{Q}_0] = 2i$, the term $H_C = (\hat{Q}_0 - q_g)^2 / (2C_{\text{SC}})$ describes the Coulomb charging energy of the SC due to the capacitance C_{SC} . The offset charge q_g can be controlled by a gate voltage. Finally, the charge and spin of an edge segment are given by

$$\left. \begin{array}{l} \hat{Q}_{AB} \\ \hat{S}_{AB} \end{array} \right\} = \int_A^B dx (\hat{\rho}_{\uparrow} \pm \hat{\rho}_{\downarrow}), \quad \hat{\rho}_s(x) = \frac{s\sqrt{\nu}}{2\pi} \partial_x \hat{\phi}_s. \quad (3)$$

A parafermion N -box is then defined by $N + 1$ FM and N SC domains excluding the outer edges. For instance, Fig. 1 shows a 2-box.

Low-energy theory.—The quasiparticle excitations in the SC and FM domains have a gap $(4\pi v \Delta / \nu)^{1/2}$ and $(4\pi v t / \nu)^{1/2}$ respectively [16]. At energies below these scales, the problem can be simplified using the method of Ref. [40], since the large cosines in Eqs. (1) and (2) imply that each FM (SC) domain is then effectively described by an integer-valued operator \hat{m}_j (\hat{n}_j), see Refs. [16, 18] and Fig. 1(a),

$$\left. \frac{\hat{\phi}_{\uparrow}(x) \mp \hat{\phi}_{\downarrow}(x)}{2\pi\sqrt{\nu}} \right|_{x \in \text{FM}_j / \text{SC}_j} = \begin{cases} \hat{m}_j, \\ \hat{n}_j - \hat{\varphi} / (2\pi). \end{cases} \quad (4)$$

The only non-trivial commutation relation is $[\hat{m}_j, \hat{n}_l] = i/(\pi\nu)$ for $j > l$, while $[\hat{m}_j, \hat{n}_l] = 0$ for $j \leq l$. Using Eq. (3), the charge \hat{Q}_j (spin \hat{S}_j) of the edge segment corresponding to SC_j (FM_j except for the first and the last FM) is

$$\hat{Q}_j = \nu(\hat{m}_{j+1} - \hat{m}_j), \quad \hat{S}_j = \nu(\hat{n}_j - \hat{n}_{j-1}). \quad (5)$$

Note that FM (SC) domains cannot host charge (spin) at low energies. The semi-infinite outer edges are merged with each other and decouple from the PF box. We will probe the system by tunneling of fractional quasiparticles below. At low energies, this can only happen at interfaces between different domains. The projected low-energy quasiparticle operators are given by, cf. Refs. [16, 18],

$$\hat{\alpha}_{j,s} = \begin{cases} e^{i\pi\nu(\hat{n}_l + s\hat{m}_l - \hat{\varphi}/2\pi)}, & j = 2l - 1, \\ e^{i\pi\nu(\hat{n}_l + s\hat{m}_{l+1} - \hat{\varphi}/2\pi)}, & j = 2l, \end{cases} \quad (6)$$

where j is the domain wall number and s the spin of the edge, see Fig. 1(a). The PF operators in Eq. (6) satisfy a \mathbb{Z}_n parafermion algebra with index $n = 2/\nu$ [29],

$$\hat{\alpha}_{j,s} \hat{\alpha}_{l,s} = \omega_s^{\text{sgn}(l-j)} \hat{\alpha}_{l,s} \hat{\alpha}_{j,s}, \quad \omega_s = e^{2\pi i s / n} = e^{i\pi \nu s}. \quad (7)$$

The low-energy Hilbert space of the box is now spanned by $|Q_{\text{tot}}, Q_{j=1, \dots, N-1} \pmod{2}\rangle$, where $\hat{Q}_{\text{tot}} = \sum_{j=0}^N \hat{Q}_j = \hat{Q}_0 + \nu(\hat{m}_{N+1} - \hat{m}_1)$ is the total charge of the proximitizing SC and the FQH edges within the PF box. Note that Q_{tot} has fractional values differing by multiples of ν . Since the SC can absorb electron pairs, the remaining quantum numbers describe the distribution of fractional quasiparticles over the SC domains of the PF box. The box Hamiltonian is then given by

$$H_{\text{box}} = \frac{1}{2C_{\text{box}}} (\hat{Q}_{\text{tot}} - q_g)^2, \quad (8)$$

where C_{box} is the effective box capacitance and all states with the same Q_{tot} are degenerate to exponential accuracy [33]. In what follows we ignore the consequent tiny residual splittings and focus on the simplest configurations, namely the 1-box and the 2-box. The Hilbert space of the 1-box is spanned by $|Q_{\text{tot}}\rangle$ and does not allow for a degenerate subspace. In contrast, for every value of Q_{tot} , the 2-box has topological degeneracy $n = 2/\nu$ due to the different ways to distribute charge between SC_1 and SC_2 .

Cotunneling Hamiltonian with FQH edges.—We next consider two additional edge segments ($\gamma = 1, 2$), each approaching (near $x = x_\gamma$) a PF zero mode on the box. Such edges serve as leads and correspond to fields $\hat{\phi}_\gamma(x)$ with $[\hat{\phi}_\gamma(x), \hat{\phi}_\gamma(x')] = i\chi\pi\text{sgn}(x - x')$, where $\chi = \pm 1$ is the edge chirality. With applied voltage V_γ , the edge Hamiltonian is given by $H_\gamma = H_{\text{edge}}[\hat{\phi}_\gamma] - \frac{\chi\sqrt{\nu}}{2\pi} V_\gamma \int dx \partial_x \hat{\phi}_\gamma$. Quasiparticles can then tunnel with amplitude η_γ between the edge and the PF $\hat{\alpha}_{j,s}$, which is modeled by the tunneling Hamiltonian $H_T = \sum_{\gamma=1,2} \eta_\gamma e^{i\sqrt{\nu}\hat{\phi}_\gamma(x_\gamma)} \hat{\alpha}_{j,s}^\dagger + \text{h.c.}$, see Fig. 2.

We now assume that the box charging energy in Eq. (8) is the largest energy scale. Away from Coulomb resonances, $q_g \neq \nu(\mathbb{Z} + 1/2)$, transport between two leads is then dominated by cotunneling. By projecting to the Q_{tot} state minimizing the charging energy, $H_{\text{box}} + H_T \rightarrow H_{T12}$, we obtain

$$H_{T12} = \hat{\eta}_{T12} e^{-i\sqrt{\nu}\hat{\phi}_2(x_2)} e^{i\sqrt{\nu}\hat{\phi}_1(x_1)} + \text{h.c.}, \quad (9)$$

$$\hat{\eta}_{T12} = \eta_{\text{ref}} + \eta_{\text{cot}} \hat{\alpha}_{j_2,s} \hat{\alpha}_{j_1,s}^\dagger,$$

where $\eta_{\text{cot}} = \eta_1 \eta_2^* (U_+^{-1} + U_-^{-1})$ with the charging energy U_+ (U_-) for adding (removing) one fractional quasiparticle to (from) the box. In addition, we included a reference arm with amplitude η_{ref} which describes direct quasiparticle tunneling between the leads, see Fig. 2. Since the operator $\hat{\alpha}_{j_2,s} \hat{\alpha}_{j_1,s}^\dagger$ in Eq. (9) acts only in the discrete box subspace, the effective cotunneling Hamiltonian H_{T12} corresponds to quasiparticle tunneling between the leads with effective amplitude $\hat{\eta}_{T12}$. Noting

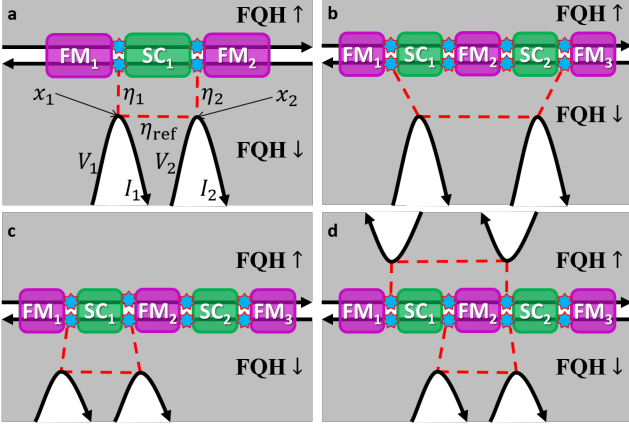


Figure 2. Setups for measuring the PF box state with additional FQH edges (curved black arrows) as leads. Tunnel couplings are indicated by dashed red lines. Panel (a) illustrates how to measure $\hat{Q}_{\text{tot}} \bmod 2$ in a 1-box. Panels (b,c,d) show setups for measuring various observables in a 2-box: $(\hat{Q}_{\text{tot}} - \hat{S}_2) \bmod 2$ [(b)]; $\hat{Q}_1 \bmod 2$ [(c)]; $(\hat{S}_2 - \hat{Q}_1) \bmod 2$ and $\hat{S}_2 \bmod 2$ for the upper and lower pair of leads, respectively [(d)].

that $(\hat{\alpha}_{j_2,s} \hat{\alpha}_{j_1,s}^\dagger)^n = e^{i\delta\varphi}$ with $n = 2/\nu$ and $\delta\varphi = \pi$ [41], the properties specific to PFs are here encoded by the cotunneling phase. Indeed, the eigenvalues of $\hat{\alpha}_{j_2,s} \hat{\alpha}_{j_1,s}^\dagger$ follow as $e^{i\nu(\pi r + \delta\varphi/2)}$ (integer r), and the cotunneling phase therefore depends on the PF box state with possible phase values differing by multiples of $\pi\nu$.

Cotunneling current.—Next we observe that H_{T12} is relevant under the renormalization group (RG), with scaling dimension equal to $\nu < 1$. The RG flow towards the strong quasiparticle tunneling regime eventually implies a two-terminal conductance $\nu e^2/h$ [28]. However, for a finite voltage $V_{12} = V_1 - V_2$ with $|V_{12}| \gg V_B \propto |\eta_{T12}|^{1/(1-\nu)}$, the RG flow is effectively cut off. For a given V_{12} , this regime is always realized for sufficiently small tunnel couplings. The tunneling current, $I_{T12} = I_2 - \nu e^2 V_2/h$, between the two leads then follows from perturbation theory in H_{T12} [42],

$$\hat{I}_{T12} = \frac{|\hat{\eta}_{T12}|^2}{v^{2\nu}} \frac{2\pi\nu}{\Gamma(2\nu)} (\nu|V_{12}|)^{2\nu-1} \text{sgn}(V_{12}). \quad (10)$$

For a box initially in a superposition of different $\hat{\alpha}_{j_2,s} \hat{\alpha}_{j_1,s}^\dagger$ eigenstates, such a current measurement implies a projection to the observed eigenstate, cf. Refs. [9, 12]. By measuring \hat{I}_{T12} and hence $|\hat{\eta}_{T12}|$, one can therefore characterize the quantum state of a PF box.

Number of eigenvalues.—Consider the configuration in Fig. 2(a), which gives access to the operator $\hat{\alpha}_{2,\downarrow} \hat{\alpha}_{1,\downarrow}^\dagger = e^{-i\pi(\hat{Q}_{\text{tot}} + \nu/2)}$, cf. Eqs. (6) and (9), via two leads connected to a 1-box. We now tune the box to a Coulomb blockade valley. By varying the backgate voltage across a peak, $q_g \rightarrow q_g + \nu$, we also enforce $Q_{\text{tot}} \rightarrow Q_{\text{tot}} + \nu$,

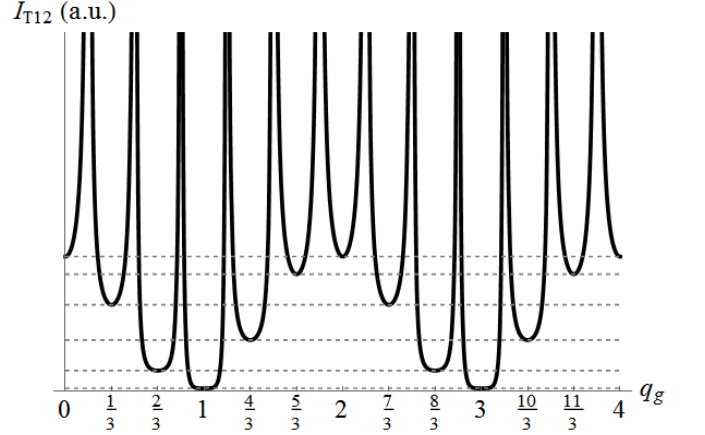


Figure 3. Sketch of the tunneling current I_{T12} vs. gate parameter q_g for the 1-box configuration in Fig. 2(a) with $\nu = 1/3$. The current in a Coulomb valley depends on $Q_{\text{tot}} \bmod 2$ and thus on q_g . When gradually increasing $q_g \rightarrow q_g + 2$, one passes through $n = 2/\nu$ peaks with much larger (yet finite) current. At the end of this sequence, the same current I_{T12} is repeated.

since the box will adhere to the ground state of H_{box} . As a consequence, we effectively obtain $\eta_{\text{cot}} \rightarrow \eta_{\text{cot}} e^{-i\pi\nu}$ in Eq. (9), and thus a different tunneling current I_{T12} . After switching through $n = 2/\nu$ subsequent Coulomb valleys, we have $q_g \rightarrow q_g + 2$ and return to the original value of I_{T12} . This characteristic dependence of I_{T12} on q_g is sketched in Fig. 3. Such an experiment can already determine the number n of possible eigenvalues of $\hat{\alpha}_{2,\downarrow} \hat{\alpha}_{1,\downarrow}^\dagger$.

Degenerate PF space.—Next we show how to engineer an n -fold degenerate PF space. To accomplish this task, we consider a 2-box as shown in Figs. 2(b-d). The 2-box has two degrees of freedom, namely Q_{tot} , which behaves the same way as for the 1-box, and $Q_1 \bmod 2$, which labels the n -fold degenerate subspace for any given Q_{tot} . The 2-box contains four domain walls, allowing for various options to access PF operator combinations. For instance, by connecting leads to the first and the last domain wall, cf. Fig. 2(b), a current measurement determines the phase of $\hat{\alpha}_{4,s} \hat{\alpha}_{1,s}^\dagger = e^{i\pi(s\hat{Q}_{\text{tot}} + s\nu/2 + \hat{S}_2)}$. Repeating the above 1-box protocol then implies a q_g -dependent behavior as in Fig. 3 [43]. To demonstrate that the subspace for fixed Q_{tot} is in fact degenerate, we first note that it is spanned by the $|Q_1 \bmod 2\rangle$ states. These states correspond to the eigenvalues $e^{is\pi(Q_1 + \nu/2)}$ of $\hat{\alpha}_{2,s} \hat{\alpha}_{1,s}^\dagger$, which in turn follow from current measurements as shown in Fig. 2(c). Next, $\hat{\alpha}_{3,s} \hat{\alpha}_{2,s}^\dagger = e^{i\pi(\hat{S}_2 + s\nu/2)}$ and $\hat{\alpha}_{3,s} \hat{\alpha}_{1,s}^\dagger = e^{i\pi(s\hat{Q}_1 + \hat{S}_2 + s\nu/2)}$ imply that this degenerate subspace is also spanned by the eigenbasis of \hat{S}_2 , or of $\hat{S}_2 \pm \hat{Q}_1$. Both operators can be accessed as illustrated in Fig. 2(d). Now let us take any eigenstate $|Q_1 \bmod 2\rangle$ of $\hat{\alpha}_{2,s} \hat{\alpha}_{1,s}^\dagger$. Decomposing it into the eigenstates of $\hat{\alpha}_{3,s} \hat{\alpha}_{2,s}^\dagger$,

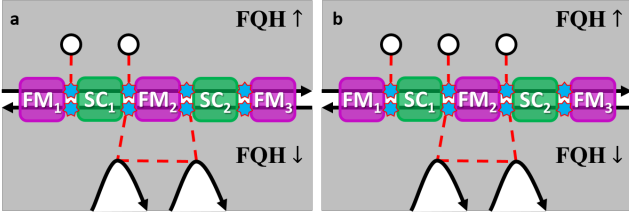


Figure 4. Setups allowing for 2-box manipulation with QADs (white circles). Panel (a) illustrates that the operator $\hat{\alpha}_{2,\uparrow}\hat{\alpha}_{1,\uparrow}^\dagger$ can be applied to an arbitrary PF box state by pumping a quasiparticle between the QAD pair. In the same setup, $\hat{S}_2 \bmod 2$ can be measured from the tunneling current between the shown leads. Panel (b) presents a setup allowing for application of operations $\hat{\alpha}_{2,\uparrow}\hat{\alpha}_{1,\uparrow}^\dagger$ and $\hat{\alpha}_{3,\uparrow}\hat{\alpha}_{2,\uparrow}^\dagger$, which is sufficient to generate any digital operation that can be applied through QADs, and measuring $\hat{S}_2 \bmod 2$.

we obtain

$$|Q_1 \bmod 2\rangle = \frac{1}{\sqrt{n}} \sum_{r=0}^{n-1} e^{i\pi\lambda_r} |(S_2 \bmod 2) = \nu r\rangle, \quad (11)$$

where $\lambda_r = r(Q_1 \bmod 2)$. Similar statements hold for any pair of the above observables. This structure allows one to confirm the degeneracy of the subspace.

Indeed, let us select an arbitrary pair of non-commuting bilinear PF operators, e.g., $\hat{O}_1 = \hat{\alpha}_{2,\uparrow}\hat{\alpha}_{1,\uparrow}^\dagger$ and $\hat{O}_2 = \hat{\alpha}_{3,\uparrow}\hat{\alpha}_{2,\uparrow}^\dagger$. A measurement of \hat{O}_1 now projects the box state onto one of its n eigenstates. Then one measures \hat{O}_2 , which should project the system with equal probabilities, see Eq. (11), onto any eigenstate of \hat{O}_2 . Similarly, a subsequent measurement of \hat{O}_1 projects this state with equal probabilities onto one of the eigenstates of \hat{O}_1 . Repeating this procedure many times, one can verify that \hat{O}_1 (or \hat{O}_2) has precisely n possible eigenvalues. To explicitly check the degeneracy one may now proceed as follows. One first performs repetitive measurements of \hat{O}_1 , with arbitrary time intervals between consecutive current measurements. If we always find the same eigenvalue, we know that $[\hat{O}_1, H_{\text{box}}] = 0$. Now repeat this procedure for the operator \hat{O}_2 , which does not commute with \hat{O}_1 . If we also find $[\hat{O}_2, H_{\text{box}}] = 0$, all eigenstates of both \hat{O}_1 and \hat{O}_2 have trivial time evolution, which proves the degeneracy of the PF space.

PF state manipulation.—Finally we discuss how to perform on-demand transitions in the n -fold degenerate subspace of a 2-box with quantum anti-dots (QADs) surrounded by the FQH liquid [44–48] as access units, see Fig. 4. At low energy scales, a QAD in the Coulomb blockade regime is equivalent to a two-level system,

$$H_{\text{QAD}} = \nu V_{\text{QAD}} \left(\hat{\psi}_{\text{QAD}}^\dagger \hat{\psi}_{\text{QAD}} - \frac{1}{2} \right) = \frac{V_{\text{QAD}}}{n} \begin{pmatrix} 1 & 0 \\ 0 & -1 \end{pmatrix}, \quad (12)$$

where V_{QAD} is an electrostatic gate potential and $\hat{\psi}_{\text{QAD}}$ the quasiparticle annihilation operator on the QAD. Consider now two QADs coupled to the 2-box as in Fig. 4(a). Similarly to Eq. (9), elastic cotunneling between two QADs via the PF box is described by $H_{\text{cot,QAD}} = \eta_{\text{cot}} \hat{\psi}_{\text{QAD}2}^\dagger \hat{\psi}_{\text{QAD}1} \hat{\alpha}_{j2,s} \hat{\alpha}_{j1,s}^\dagger + \text{h.c.}$, where the amplitude η_{cot} now does not renormalize anymore. By adiabatically pumping a quasiparticle from QAD1 to QAD2 through suitable changes of the gate voltages $V_{\text{QAD}1/2}$, an arbitrary PF box state $|\Phi\rangle$ must then transform according to $|\Phi\rangle \rightarrow \hat{\alpha}_{j2,s} \hat{\alpha}_{j1,s}^\dagger |\Phi\rangle$, independent of microscopic details of the protocol, see Refs. [9, 12] for the simpler $\nu = 1$ case. In this way, QADs make it possible to perform digital operations $\hat{\alpha}_{j,s} \hat{\alpha}_{l,s}^\dagger$ within the degenerate PF state manifold. For example, the configuration in Fig. 4(a) permits to measure $\hat{\alpha}_{3,\downarrow} \hat{\alpha}_{2,\downarrow}^\dagger = e^{i\pi(\hat{S}_2 - \nu/2)}$ through the cotunneling current via attached leads. At the same time, this setup facilitates the application of the operator $\hat{\alpha}_{2,\uparrow} \hat{\alpha}_{1,\uparrow}^\dagger = e^{i\pi(\hat{Q}_1 + \nu/2)}$ by employing the indicated pair of QADs. From Eq. (6) we can now show that application of the operator $\hat{\alpha}_{2,\uparrow} \hat{\alpha}_{1,\uparrow}^\dagger$ changes $\hat{S}_2 \rightarrow \hat{S}_2 - \nu \pmod{2}$. By exploiting this setup, one can therefore map out the 2-box degenerate Hilbert space dimension and switch between different eigenstates in a controlled manner. We emphasize that all non-trivial digital operations can already be generated by using two operators, e.g., $\hat{\alpha}_{2,\uparrow} \hat{\alpha}_{1,\uparrow}^\dagger$ and $\hat{\alpha}_{3,\uparrow} \hat{\alpha}_{2,\uparrow}^\dagger$. Such operators may be realized by employing three QADs, see Fig. 4(b). With the handles specified above, it follows that one can experimentally test the PF algebra in Eq. (7).

Conclusions.—The parafermion box introduced in this work can simplify and facilitate experimental studies of PF-based quantum states. Our proposed measurement protocols, which employ fractional edge states as leads and/or quantum anti-dots for state manipulation, crucially rely on the unique and intrinsically non-local ways to access the box in the Coulomb blockade regime. One can thereby largely avoid several difficulties that may affect earlier proposals for observing PF physics. In particular, we have shown how to observe the dimension of the zero-mode space, how to realize and demonstrate the existence of a degenerate space, and how to perform digital operations in this degenerate state manifold. The results of our protocols are distinctly different from Coulomb blockade signatures of anyonic tunneling and should enable the experimental confirmation of the parafermion algebra in Eq. (7).

We thank A. Altland and K. Flensberg for discussions. We acknowledge funding by the Deutsche Forschungsgemeinschaft (Bonn) within the network CRC TR 183 (project C01) and Grant No. RO 2247/8-1, by the IMOS Israel-Russia program, and by the ISF. This text was prepared with the help of the LyX software [49].

-
- [1] C. Nayak, S.H. Simon, A. Stern, M. Freedman, and S. Das Sarma, *Rev. Mod. Phys.* **80**, 1083 (2008).
- [2] J. Alicea, *Rep. Prog. Phys.* **75**, 076501 (2012).
- [3] M. Leijnse and K. Flensberg, *Semicond. Sci. Techn.* **27**, 124003 (2012).
- [4] C.W.J. Beenakker, *Annu. Rev. Condens. Matt. Phys.* **4**, 113 (2013).
- [5] L. Fu, *Phys. Rev. Lett.* **104**, 056402 (2010).
- [6] B. Béri and N.R. Cooper, *Phys. Rev. Lett.* **109**, 156803 (2012).
- [7] A. Altland and R. Egger, *Phys. Rev. Lett.* **110**, 196401 (2013).
- [8] B. Béri, *Phys. Rev. Lett.* **110**, 216803 (2013).
- [9] L.A. Landau, S. Plugge, E. Sela, A. Altland, S.M. Albrecht, and R. Egger, *Phys. Rev. Lett.* **116**, 050501 (2016).
- [10] D. Aasen *et al.*, *Phys. Rev. X* **6**, 031016 (2016).
- [11] S. Vijay and L. Fu, *Phys. Rev. B* **94**, 235446 (2016).
- [12] S. Plugge, A. Rasmussen, R. Egger, and K. Flensberg, *New J. Phys.* **19**, 012001 (2017).
- [13] T. Karzig *et al.*, preprint arXiv:1610.05289.
- [14] S.M. Albrecht, A.P. Higginbotham, M. Madsen, F. Kuemmeth, T.S. Jespersen, J. Nygård, P. Krogstrup, and C.M. Marcus, *Nature* **531**, 206 (2016).
- [15] S.M. Albrecht, E.B. Hansen, A.P. Higginbotham, F. Kuemmeth, T.S. Jespersen, J. Nygård, P. Krogstrup, J. Danon, K. Flensberg, and C.M. Marcus, *Phys. Rev. Lett.* **118**, 137701 (2017).
- [16] N.H. Lindner, E. Berg, G. Refael, and A. Stern, *Phys. Rev. X* **2**, 041002 (2012).
- [17] M. Cheng, *Phys. Rev. B* **86**, 195126 (2012).
- [18] D.J. Clarke, J. Alicea, and K. Shtengel, *Nature Commun.* **4**, 1348 (2013).
- [19] M. Burrello, B. van Heck, and E. Cobanera, *Phys. Rev. B* **87**, 195422 (2013).
- [20] A. Vaezi, *Phys. Rev. B* **87**, 035132 (2013).
- [21] F. Zhang and C.L. Kane, *Phys. Rev. Lett.* **113**, 036401 (2014).
- [22] R.S.K. Mong *et al.*, *Phys. Rev. X* **4**, 011036 (2014).
- [23] D.J. Clarke, J. Alicea, and K. Shtengel, *Nature Phys.* **10**, 877 (2014).
- [24] M. Barkeshli, Y. Oreg, and X.L. Qi, arXiv:1401.3750.
- [25] M. Barkeshli and X.L. Qi, *Phys. Rev. X* **4**, 041035 (2014).
- [26] M. Cheng and R.M. Lutchyn, *Phys. Rev. B* **92**, 134516 (2015).
- [27] J. Alicea and A. Stern, *Phys. Scr.* **T164**, 14006 (2015).
- [28] Y. Kim, D.J. Clarke, and R.M. Lutchyn, arXiv:1703.00498.
- [29] J. Alicea and P. Fendley, *Annu. Rev. Condens. Matter Phys.* **7**, 119 (2016).
- [30] L. Fidkowski and A. Kitaev, *Phys. Rev. B* **83**, 075103 (2011).
- [31] J. Klinovaja and D. Loss, *Phys. Rev. Lett.* **112**, 246403 (2014).
- [32] For example, relaxation to the lowest energy state of a junction with multiple Josephson periodicity, e.g., by quasiparticle poisoning mechanisms, can restore the conventional 2π periodicity [18]. Moreover, the proposed observation of conductance $\nu e^2/h$ when charging energy is present [28] can at best reveal the fractional charge and the scaling dimension of quasiparticles in the leads, but tells us nothing specific about PFs.
- [33] See the accompanying Supplemental Material, where we provide additional details on the charging Hamiltonian, on measurement protocols, and discuss the applicability of our results to the $\nu = 2/3$ platform. This includes citations of [34–38].
- [34] M. Barkeshli, *Phys. Rev. Lett.* **117**, 096803 (2016).
- [35] C.L. Kane, M.P.A. Fisher, and J. Polchinski, *Phys. Rev. Lett.* **72**, 4129 (1994).
- [36] C.L. Kane and M.P.A. Fisher, *Phys. Rev. B* **51**, 13449 (1995).
- [37] J. Wang, Y. Meir, and Y. Gefen, *Phys. Rev. Lett.* **111**, 246803 (2013).
- [38] I.V. Protopopov, Y. Gefen, A.D. Mirlin, arXiv:1703.02746.
- [39] By introducing a magnetic field component in the y -direction, cf. Fig. 1(b), one can separately control the phase of each SC domain, $\hat{\varphi} \rightarrow \hat{\varphi} + \varphi_j$, see Ref. [33].
- [40] S. Ganeshan and M. Levin, *Phys. Rev. B* **93**, 075118 (2016).
- [41] When SC order parameter phases differ between domains, we find $\delta\varphi = \pi + \varphi_{[(j_1+1)/2]} - \varphi_{[(j_2+1)/2]}$, where $[x]$ is the integer part of x .
- [42] X.G. Wen, *Phys. Rev. B* **44**, 5708 (1991).
- [43] Here, however, one has an additional knob for tuning the relative phase between the reference arm and the cotunneling path. This can be achieved by tuning the SC phase difference $\varphi_2 - \varphi_1$, which modifies the eigenvalues of \hat{S}_2 compared to Eq. (5), $\hat{S}_2 = \nu(\hat{n}_2 - \hat{n}_1) - \nu(\varphi_2 - \varphi_1)/2\pi$.
- [44] S. Kivelson and V.L. Pokrovsky, *Phys. Rev. B* **40**, 1373 (1989).
- [45] S. Kivelson, *Phys. Rev. Lett.* **65**, 3369 (1990).
- [46] V.J. Goldman, *Surf. Sci.* **361-362**, 1 (1996).
- [47] V.J. Goldman, *Physica E* **1**, 15 (1997).
- [48] I.J. Maasilta and V.J. Goldman, *Phys. Rev. B* **55**, 4081 (1997).
- [49] The LyX Team. LyX 2.2.2 – The Document Processor [Computer software and manual], <http://www.lyx.org>, 2016.

Supplemental Material to “Measurement and Control of Coulomb-Blockaded Parafermion Box”

Kyrylo Snizhko,¹ Reinhold Egger,² and Yuval Gefen¹

¹*Department of Condensed Matter Physics, Weizmann Institute of Science, Rehovot, 76100 Israel*

²*Institut für Theoretische Physik, Heinrich-Heine-Universität, D-40225 Düsseldorf, Germany*

(Dated: April 11, 2017)

In this Supplemental Material we discuss some technical aspects of our model and the applicability of our results to the $\nu = 2/3$ platform for parafermions. Sec. I discusses how our model for the parafermion box changes when there are order parameter phase differences between the SC domains, and how these phase differences can be usefully utilized. Sec. II provides technical details regarding the derivation of the box charging energy. In Sec. III, we elaborate on how the two-lead measurement scheme implements a projective measurement. In Sec. IV, the relation between the eigenbases of different observables acting in the 2-box degenerate subspace is derived. Sec. V elaborates on the protocol for manipulating an N -box degenerate subspace via QADs. Finally, Sec. VI discusses the applicability of our results to parafermions generated on the boundaries of $\nu = 2/3$ puddles.

I. NON-UNIFORM SC ORDER PARAMETER

An additional control handle can be brought to the PF box setup discussed in the main text through enabling the order parameter of different SC domains to have different phases. This can be done via applying a magnetic field in the y direction (cf. Fig. S1). The SC proximitizing Hamiltonian then becomes

$$H_{SC} = -\Delta \sum_{j=1}^N \int_{SC_j} dx \cos \left(\frac{\hat{\phi}_{\uparrow}(x) + \hat{\phi}_{\downarrow}(x)}{\sqrt{\nu}} + \hat{\varphi}_j \right), \quad (S1)$$

where $\hat{\varphi}_j = \hat{\varphi} + \varphi_j$, $\hat{\varphi}$ is the bulk SC phase operator, and $\{\varphi_j\}$ are the phase differences between the domains and the bulk SC due to the fact that the system is subject to the magnetic field B_y . As a result of this modification, the expressions for the corresponding box operators become:

$$\frac{\hat{\phi}_{\uparrow}(x) \mp \hat{\phi}_{\downarrow}(x)}{2\pi\sqrt{\nu}} \Big|_{x \in FM_j/SC_j} = \begin{cases} \hat{n}_j, \\ \hat{n}_j - \hat{\varphi}_j/(2\pi). \end{cases}, \quad (S2)$$

$$\hat{Q}_j = \nu(\hat{n}_{j+1} - \hat{n}_j), \quad (S3)$$

$$\hat{S}_j = \nu(\hat{n}_j - \hat{n}_{j-1}) - \nu(\hat{\varphi}_j - \hat{\varphi}_{j-1})/(2\pi), \quad (S4)$$

$$\hat{\alpha}_{j,s} = \begin{cases} e^{i\pi\nu(\hat{n}_l + s\hat{m}_l - \hat{\varphi}_l/2\pi)}, & j = 2l - 1, \\ e^{i\pi\nu(\hat{n}_l + s\hat{m}_{l+1} - \hat{\varphi}_l/2\pi)}, & j = 2l. \end{cases} \quad (S5)$$

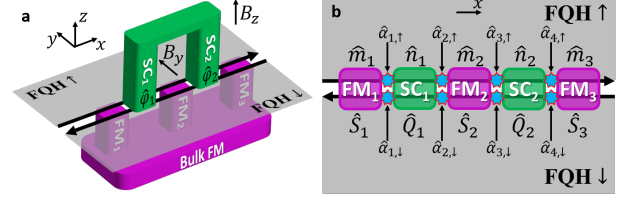


Figure S1. *The layout of a PF box with applied B_y magnetic field. a – The application of B_y magnetic field creates phase difference between different SC domains. b – The physical structure of the PF box remains the same as for $B_y = 0$. However, the expressions for operators \hat{n}_j , \hat{S}_j , and $\hat{\alpha}_{j,s}$ [cf. Eqs. (4-6)] are somewhat modified, see Eqs. (S2-S5).*

See Eqs. (4-6) in the main text for corresponding expressions at $B_y = 0$.

The tunability of the phase differences $\varphi_j - \varphi_l$ is advantageous in the protocol for measuring the box operators proposed in the main text (cf. Fig. 2 and Eqs. (9-10)): one may control the interference phase in $\hat{\eta}_{T12} = \eta_{\text{ref}} + \eta_{\text{cot}} \hat{\alpha}_{j_2,s} \hat{\alpha}_{j_1,s}^\dagger$ in order to produce optimal conditions for distinguishing different box states whenever the two parafermionic operators $\hat{\alpha}_{j_1,s}$, $\hat{\alpha}_{j_2,s}$ belong to different SC domains. Note that while a similar effect can be achieved by varying B_z and thus adjusting directly the phase difference between η_{ref} and η_{cot} through Aharonov-Bohm effect, varying the perpendicular field would have the unwanted side effect of influencing the FQH liquids.

II. THE CHARGING ENERGY OF THE PARA-FERMIONIC BOXES

Here we provide technical details about the derivation of the low-energy theory of the PF box model, putting special emphasis on the role of the charging energy. In the limit $\Delta, t \rightarrow +\infty$ the fields tend to be pinned to the cosine minima, see Eqs. (1,2) of the main text. Expanding the cosines near their minima one can show for each domain that the finite momentum excitations in the domains are gapped (see, e.g., Appendix A1 of Ref. [1]). Therefore, at low energies the cosine arguments in Eqs. (1,2) of the main text are constant within the respective domains. In this approximation, imposing continuity of the fields

$\hat{\phi}_s(x)$, one obtains for $\hat{\theta}_\pm(x) = \hat{\phi}_\uparrow(x) \pm \hat{\phi}_\downarrow(x)$

$$\hat{\theta}_+(x) = \begin{cases} 2\pi\sqrt{\nu}\hat{n}_j - \sqrt{\nu}\hat{\varphi} & , x \in \text{SC}_j, \\ \frac{2\pi(x-x_{2j-2})}{\sqrt{\nu}L_{\text{FM}}}\hat{S}_j + \hat{\theta}_+(x_{2j-2}^-) & , x \in \text{FM}_j, \end{cases} \quad (\text{S6})$$

$$\hat{\theta}_-(x) = \begin{cases} 2\pi\sqrt{\nu}\hat{n}_j & , x \in \text{FM}_j, \\ \frac{2\pi(x-x_{2j-1})}{\sqrt{\nu}L_{\text{SC}}}\hat{Q}_j + \hat{\theta}_-(x_{2j-1}^-) & , x \in \text{SC}_j, \end{cases} \quad (\text{S7})$$

where $L_{\text{FM/SC}}$ is the length of the respective domain, x_j is the coordinate of the j th domain wall (x_0 and x_{2N+1} correspond to the left edge of FM_1 and the right edge of FM_{N+1} respectively), x_j^- is infinitesimally close to x_j on the left, $\hat{Q}_j = \nu(\hat{n}_{j+1} - \hat{n}_j)$ and $\hat{S}_j = \nu(\hat{n}_j - \hat{n}_{j-1})$ are respectively the charge (spin) of the edge segment under SC_j (FM_j), and $\hat{\varphi}$ is the proximitizing SC order parameter phase. For the first and last FM domains the expression for the hosted spin is different:

$$\hat{S}_1 = \left(\nu\hat{n}_1 - \frac{\nu\hat{\varphi}}{2\pi} \right) - \frac{\sqrt{\nu}}{2\pi}\hat{\theta}_+(x_0), \quad (\text{S8})$$

$$\hat{S}_{N+1} = \frac{\sqrt{\nu}}{2\pi}\hat{\theta}_+(x_{2N+1}) - \left(\nu\hat{n}_N - \frac{\nu\hat{\varphi}}{2\pi} \right). \quad (\text{S9})$$

The commutation relations obeyed by the operators can be deduced from the commutation relations for $\hat{\phi}_\uparrow(x)$, $\hat{\phi}_\downarrow(x)$, and their derivatives; the non-trivial commutations are:

$$[\hat{m}_j, \hat{n}_l] = \begin{cases} \frac{i}{\pi\nu} & , j > l, \\ 0 & , j \leq l, \end{cases} \quad (\text{S10})$$

$$[\hat{Q}_j, \hat{n}_l] = [\hat{S}_j, \hat{m}_l] = \frac{i}{\pi}\delta_{jl}, \quad (\text{S11})$$

$$[\hat{Q}_j, \hat{S}_l] = \frac{i\nu}{\pi}(\delta_{jl} - \delta_{j+1,l}), \quad (\text{S12})$$

$$[\hat{Q}_0, \hat{n}_j] = -\frac{i}{\pi}, \quad j, l \geq 1. \quad (\text{S13})$$

The system Hamiltonian then acquires the form

$$H = \sum_{\text{FM}} \left(\frac{\pi v}{2\nu L_{\text{FM}}} \hat{S}_j^2 - t L_{\text{FM}} \cos(2\pi \hat{m}_j) \right) + \sum_{\text{SC}} \left(\frac{\pi v}{2\nu L_{\text{SC}}} \hat{Q}_j^2 - \Delta L_{\text{SC}} \cos(2\pi \hat{n}_j) \right) + \frac{(\hat{Q}_0 - q_g)^2}{2C_{\text{SC}}} + \text{semi-infinite edges}. \quad (\text{S14})$$

A system described by the first two terms on the r.h.s. of (S14) has been considered in Ref. [1], and the semi-infinite edges in conjunction with such a system have been considered in Refs. [2, 3]. The bulk SC charging energy, which appears in the third term of (S14), is a key ingredient giving rise to the box charging energy, see Eq. (8) of the main text. To the best of our knowledge, it has not been derived in previous works. We note, however, that several recent works [4, 5] have invoked a charging energy as in Eq. (8) of the main text.

An algorithm for finding the low-energy theory for Hamiltonians with large cosine terms as in Eq. (S14) has been put forward in Ref. [6] and we employ it for the analysis presented in Sec. II.3. However, before addressing the problem in its full complexity, it is instructive to consider two toy problems, which we do below.

II.1. Toy problem 1

Consider a quantum-mechanical problem with

$$H_1 = \frac{\hat{p}^2}{2m} + \frac{K\hat{x}^2}{2} - U_p \cos(2\pi\hat{p}) - U_x \cos(2\pi\hat{x}), \quad (\text{S15})$$

$$[\hat{p}, \hat{x}] = \frac{i}{\pi\nu} \quad (\text{S16})$$

with ν^{-1} being integer. H_1 is an illustrative simplification of the first two rows in (S14). First, we solve it ignoring the two middle terms.

$$H_0 = \frac{\hat{p}^2}{2m} - U_x \cos(2\pi\hat{x}). \quad (\text{S17})$$

Due to Bloch's theorem, the eigenfunctions of H_0 satisfy

$$e^{i\pi\nu\hat{p}}\psi_{kn}(x) = \psi_{kn}(x-1) = e^{-ik}\psi_{kn}(x), \quad (\text{S18})$$

where $k \in [0, 2\pi)$ is the quasi-momentum, $n \in \mathbb{Z}_+$ is the band index, and the eigenfunctions can be written as $\psi_{kn}(x) = e^{ikx}u_{kn}(x)$ with $u_{kn}(x+1) = u_{kn}(x)$. For $U_x \rightarrow +\infty$ the potential can be considered as a set of independent cosine minima with weak tunneling between them. Expanding the cosine near its minima and calculating the tunneling between them semi-classically, one finds $u_{kn}(x) = u_n(x) + \delta u_{kn}(x)$, $E_{kn} = E_n + \delta E_{kn}$ with $E_n \approx 2\nu^{-1}\sqrt{U_x/m}(n+1/2) - U_x$ and

$$\delta u_{kn}(x), \delta E_{kn} = O\left(e^{-4\nu\sqrt{mU_x}}\right). \quad (\text{S19})$$

Since the term $U_p \cos(2\pi\hat{p})$ commutes with H_0 , it only modifies the eigenenergies $E_{kn} \rightarrow E_{kn} - U_p \cos(2\nu^{-1}k)$.

Now we look for eigenfunctions of (S15) in the form

$$\Psi_n(x) = \int_0^{2\pi} dk A(k) \psi_{k \bmod 2\pi, n}(x). \quad (\text{S20})$$

Ignoring $O\left(e^{-4\nu\sqrt{mU_x}}\right)$ terms, we obtain

$$\left(-\frac{K}{2} \partial_k^2 - U_p \cos(2\nu^{-1}k) + E_n \right) A(k) = E A(k), \quad (\text{S21})$$

supplemented by the boundary condition $A(k+2\pi) = A(k)$. In the limit $U_p \rightarrow +\infty$, employing the same technique that was used to tackle H_0 , we find that the eigenfunctions $A_{yl}(k) = e^{-iky}w_{yl}(k)$ have energies $E_{yln} = E_n + \tilde{E}_l + \delta \tilde{E}_{yl}$. Here $y = 0, 1, \dots, 2\nu^{-1} - 1$ is the quasi-coordinate, $l \in \mathbb{Z}_+$ is the band index, $w_{yl}(k + \pi\nu) =$

$w_{yl}(k) = w_l(k) + \delta w_{yl}(k)$, $\tilde{E}_l \approx 2\nu^{-1}\sqrt{KU_p}(l+1/2) - U_p$, and

$$\delta w_{yl}(x), \delta \tilde{E}_{yl} = O\left(e^{-4\nu\sqrt{U_p/K}}\right). \quad (\text{S22})$$

Ignoring exponentially small terms, the eigenfunctions satisfy

$$\Psi_{yln}(x) = \int_0^{2\pi} dk e^{ik(x-y)} w_l(k) u_n(x), \quad (\text{S23})$$

$$e^{i\pi\nu\hat{x}} \Psi_{yln}(x) = e^{i\pi\nu y} \Psi_{yln}(x), \quad (\text{S24})$$

$$e^{i\pi\nu\hat{p}} \Psi_{yln}(x) = \Psi_{y+1 \bmod 2\nu^{-1}, ln}(x), \quad (\text{S25})$$

$$H_1 \Psi_{yln}(x) = (E_n + \tilde{E}_l) \Psi_{yln}(x). \quad (\text{S26})$$

In particular, the lowest-energy subspace spanned by $\Psi_{y00}(x)$ is $2\nu^{-1}$ -fold degenerate up to corrections $O\left(e^{-4\nu\sqrt{U_p/K}}, e^{-4\nu\sqrt{mU_x}}\right)$. Alternatively, one can consider the eigenbasis of $e^{i\pi\nu\hat{p}}$:

$$\tilde{\Psi}_{r00}(x) = (2\nu^{-1})^{-1/2} \sum_y e^{-i\pi\nu r y} \Psi_{y00}(x), \quad (\text{S27})$$

$$r = 0, 1, \dots, 2\nu^{-1} - 1.$$

II.2. Toy problem 2

Consider the Hamiltonian

$$H_2 = H_1 + \frac{\hat{p}_0^2}{2m_0}, \quad (\text{S28})$$

where H_1 is defined in (S15), and \hat{p}_0 satisfies

$$[\hat{p}_0, \hat{x}] = -\frac{i}{\pi\nu}, \quad [\hat{p}_0, \hat{p}] = 0. \quad (\text{S29})$$

We note that H_1 consists of a simplification of the first two r.h.s. terms in (S14), while $\hat{p}_0^2/2m_0$ is a simplified analogue of the bulk SC charging energy term. In analogy with the SC charge, \hat{Q}_0 whose conjugate operator is $\hat{\varphi}$, for \hat{p}_0 there is a conjugate variable \hat{x}_0 : $[\hat{p}_0, \hat{x}_0] = i$. For simplicity, in the present example we consider the operator \hat{p}_0 which has a continuous unbounded spectrum. This is to be contrasted with \hat{Q}_0 , whose spectrum is discrete.

Due to the presence of the second term in (S28), one cannot directly use the solution of H_1 from the previous section. Defining

$$\hat{p}_+ = \hat{p} + \hat{p}_0, \quad [\hat{p}_+, \hat{x}] = 0, \quad (\text{S30})$$

one can rewrite

$$\frac{\hat{p}^2}{2m} + \frac{\hat{p}_0^2}{2m_0} = \frac{\hat{p}_+^2}{2m_+} + \frac{(\hat{p} - \alpha\hat{p}_+)^2}{2m_p}, \quad (\text{S31})$$

$$m_+ = m + m_0, \quad \alpha = \frac{m}{m + m_0}, \quad m_p = \alpha m_0. \quad (\text{S32})$$

Therefore,

$$H_2 = \tilde{H}_1 + \frac{\hat{p}_+^2}{2m_+}, \quad (\text{S33})$$

$$\tilde{H}_1 = \frac{(\hat{p} - \alpha\hat{p}_+)^2}{2m_p} + \frac{K\hat{x}^2}{2} - U_p \cos(2\pi\hat{p}) - U_x \cos(2\pi\hat{x}). \quad (\text{S34})$$

There are two differences between \tilde{H}_1 and H_1 : first, the renormalized m_p instead of m , and second, the $\alpha\hat{p}_+$ shift. Since $[\tilde{H}_1, \hat{p}_+] = 0$ both operators can be diagonalized simultaneously. For every eigenstate of \hat{p}_+ , with a given eigenvalue, one can diagonalize \tilde{H}_1 following the procedure of Sec. II.1. The $\alpha\hat{p}_+$ shift in Eq. (S34) leads only to exponentially small corrections. Therefore, the low-energy Hilbert space of the system is spanned by $|p_+, y\rangle$ with y labeling the exponentially degenerate ground states of \tilde{H}_1 , and the low-energy effective Hamiltonian is

$$H_{\text{eff}} = \frac{\hat{p}_+^2}{2m_+}, \quad (\text{S35})$$

where we have omitted the constant offset by the ground-state energy of \tilde{H}_1 .

II.3. Solving (S14) in the limit $t, \Delta \rightarrow +\infty$

A general algorithm for solving Hamiltonians with large cosine terms as in Eq. (S14) has been developed in Ref. [6]. According to this algorithm, the cosine arguments $\{\hat{C}_q\} = \{2\pi\hat{m}_j, 2\pi\hat{n}_j\}$ play the key role. The low-energy Hilbert space is obtained through restricting the original problem Hilbert space by demanding $\cos\hat{C}_q|\psi\rangle = |\psi\rangle$, which implies that the allowed low-energy operators are those and only those that commute with all $\cos\hat{C}_q$. The low-energy effective Hamiltonian then assumes the form

$$H_{\text{eff}} = H_0 - \frac{1}{2} \sum_{q,r} (\mathcal{M}^{-1})_{qr} \hat{\Pi}_q \hat{\Pi}_r, \quad (\text{S36})$$

where H_0 is the quadratic part of the original Hamiltonian, and the variables $\hat{\Pi}_q$, conjugate to \hat{C}_q , are

$$\hat{\Pi}_q = \frac{1}{2\pi i} \sum_r \mathcal{M}_{qr} [\hat{C}_r, H_0], \quad (\text{S37})$$

where \mathcal{M}_{qr} is defined through

$$\mathcal{M} = \mathcal{N}^{-1}, \quad \mathcal{N}_{qr} = -\frac{1}{4\pi^2} [\hat{C}_q, [\hat{C}_r, H_0]]. \quad (\text{S38})$$

Finally, the non-trivial commutation relations $[\hat{C}_q, \hat{C}_r]$ lead to a degenerate low-energy Hilbert space, while the

finite coefficients in front of the cosine terms lead to splitting between these degenerate states, as also discussed in Ref. [6].

Applying this algorithm to the two toy problems discussed in Secs. II.1, II.2, one recovers the results obtained there. We now discuss the application of this algorithm to Hamiltonian (S14). The admissible low energy operators, i.e., those that commute with all $\cos 2\pi\hat{m}_j$ and $\cos 2\pi\hat{n}_j$, are $e^{i\pi\nu\hat{m}_j}$, $e^{i\pi\nu\hat{n}_j}$, $\partial_x\hat{\phi}_{\uparrow/\downarrow}$ and $e^{i\sqrt{\nu}\hat{\phi}_{\uparrow/\downarrow}}$ operators at the semi-infinite edges, and the total box charge $\hat{Q}_{\text{tot}} = \hat{Q}_0 + \sum_{j=1}^N \hat{Q}_j$. All the other low-energy operators can be built out of these. The effective low-energy Hamiltonian is

$$H_{\text{eff}} = \frac{1}{2C_{\text{box}}} \left(\hat{Q}_{\text{tot}} - q_g \right)^2 + \sum_{s=\pm 1} \left(\int_{-\infty}^{x_0} + \int_{x_{2N+1}}^{+\infty} \right) dx (\partial_x \hat{\phi}_s)^2, \quad (\text{S39})$$

where $C_{\text{box}} = C_{\text{SC}} + N\nu L_{\text{SC}}/(\pi\nu)$. The second term in H_{eff} represents the Hamiltonian of the semi-infinite edges that are glued together by the conditions

$$\hat{\phi}_{\uparrow}(x_0) - \hat{\phi}_{\downarrow}(x_0) = 2\pi\sqrt{\nu}\hat{m}_1, \quad (\text{S40})$$

$$\hat{\phi}_{\uparrow}(x_{2N+1}) - \hat{\phi}_{\downarrow}(x_{2N+1}) = 2\pi\sqrt{\nu}\hat{m}_{N+1}. \quad (\text{S41})$$

Therefore, the fields at the edges can be redefined so that the part to the left of FM_1 is described as a free FQH edge, and the part to the right of FM_{N+1} is described as another one.

The degeneracy due to the non-commutation of \hat{m}_j , \hat{n}_j and the expression of parafermionic operators through \hat{m}_j , \hat{n}_j is described the same way as without the charging energy [1, 2]. The box states can be labeled by eigenvalues of operators $e^{i\pi\hat{Q}_j}$ and \hat{Q}_{tot} . However, now not all $(\hat{Q}_j \bmod 2)$ are independent as \hat{Q}_0 is an integer multiple of 2, thus $\prod_j e^{i\pi\hat{Q}_j} = e^{i\pi\hat{Q}_{\text{tot}}}$. Since the variables of the semi-infinite edges commute with \hat{Q}_j and \hat{Q}_{tot} , the edges decouple from the box. Therefore, the box can be described independently of the edges by the Hamiltonian in Eq. (8) of the main text. The lifting of the degeneracy is $O\left(\exp\left[-4L_{\text{SC}}\left(\frac{\nu\Delta}{\pi\nu}\right)^{1/2}\left(\frac{\pi\nu C_{\text{SC}}}{\pi\nu C_{\text{SC}} + \nu L_{\text{SC}}}\right)^{1/2}\right]\right)$, $O\left(\exp\left[-4L_{\text{FM}}\left(\frac{\nu t}{\pi\nu}\right)^{1/2}\right]\right)$.

Finally, we would like to note that similar results can be derived for a generic capacitive coupling between the box elements:

$$H_C = \frac{(\hat{Q}_0 - q_g)^2}{2C_{\text{SC}}} + \sum_{jl} \left[A_{jl}\hat{Q}_j\hat{Q}_l + B_{jl}\hat{S}_j\hat{S}_l + C_{jl}\hat{Q}_j\hat{S}_l \right] + \hat{Q}_0 \sum_j \left[d_j\hat{Q}_j + e_j\hat{S}_j \right], \quad (\text{S42})$$

with arbitrary coefficients A_{jl} , B_{jl} , C_{jl} , d_j , e_j (provided that the quadratic in charges and spins part of H_C is positive definite). In this case the low-energy expression for the box Hamiltonian, Eq. (8) of the main text, retains the same form. However, the precise expression for the box capacity C_{box} changes in this case, and the gate parameter q_g should be replaced by $q_{\text{box}} = \text{const} \times q_g$.

III. SOME DETAILS REGARDING THE TWO-LEAD MEASUREMENT SCHEME

Here we discuss how the two-lead measurement scheme discussed in the main text implements a projective measurement. We assume that H_{T12} , see Eq. (9) of the main text, is switched on at time $t = 0$. Suppose the initial state of the N -box is $|\psi\rangle = \sum_{r,\{X\}} A_{r,\{X\}} |r, \{X\}\rangle$, where $|r, \{X\}\rangle$ is a basis of the box low-energy states such that

$$\hat{\alpha}_{j2,s}\hat{\alpha}_{j1,s}^\dagger |r, \{X\}\rangle = e^{i\nu(\pi r + \delta\varphi/2)} |r, \{X\}\rangle, \quad (\text{S43})$$

and $\{X\}$ denotes all other quantum numbers labeling the box state. Below we calculate the box reduced density matrix $\hat{\rho}_{\text{box}}(t)$ as a function of time. We find that

$$\langle r, \{X\} | \hat{\rho}_{\text{box}}(t) | r', \{X'\} \rangle = A_{r',\{X'\}}^* A_{r,\{X\}} e^{-F_{rr'}(t)}, \quad (\text{S44})$$

$$\text{Re } F_{rr'}(t) = t |\eta_r - \eta_{r'}|^2 \nu^{-2\nu} \frac{\pi(\nu|V_{12}|)^{2\nu-1}}{\Gamma(2\nu)}, \quad (\text{S45})$$

where $\eta_r = \eta_{\text{ref}} + \eta_{\text{cot}} e^{i\nu(\pi r + \delta\varphi/2)}$, $\Gamma(x)$ is the Euler gamma function, and the last expression is valid for $t \gg 1/(\nu|V_{12}|)$. Therefore, the scheme kills the density matrix elements that are off-diagonal in r while preserving coherent superposition in the rest of quantum numbers, thus implementing a projective measurement of r .

The derivation of the above result is as follows. Evolution of the leads and box state can be described in the interaction representation by evolution operator

$$\hat{U}(t) = T \exp \left(-i \int_0^t dt H_{\text{T12}} \right). \quad (\text{S46})$$

The initial density matrix of the system is $\hat{\rho}(t=0) = \hat{\rho}_{\text{box}}(0) \otimes \hat{\rho}_{\text{leads}}(0)$ with $\hat{\rho}_{\text{box}}(0) = |\psi\rangle\langle\psi|$ and $\hat{\rho}_{\text{leads}}(0) \sim \exp\left(-\sum_{i=1,2} H_i/T\right)$, where H_i are the leads' Hamiltonians and T is the system temperature. Therefore, the reduced density matrix of the box at time t is

$$\begin{aligned} \hat{\rho}_{\text{box}}(t) &= \text{Tr}_{\text{leads}} \left[\hat{U}(t) \hat{\rho}(0) \hat{U}^\dagger(t) \right] \\ &= \sum_{r,r'} \sum_{\{X\},\{X'\}} |r, \{X\}\rangle \langle r', \{X'\}| \\ &\quad \times A_{r',\{X'\}}^* A_{r,\{X\}} \langle U_{r'}^\dagger(t) U_r(t) \rangle_{\text{leads}}, \end{aligned} \quad (\text{S47})$$

where $U_r(t)$ is obtained from $\hat{U}(t)$ by substituting $\hat{\alpha}_{j_2,s}\hat{\alpha}_{j_1,s}^\dagger$ in H_{T12} with its eigenvalue (S43). We define

$$F_{rr'}(t) = -\ln\langle U_{r'}^\dagger(t)U_r(t)\rangle_{\text{leads}}. \quad (\text{S48})$$

Since $U_r^\dagger(t)U_r(t) = 1$, $F_{rr}(t) = 0$. For the off-diagonal components we perform a second order cumulant expansion in H_{T12} and obtain

$$\text{Re } F_{rr'}(t) = 2|\eta_r - \eta_{r'}|^2 v^{-2\nu} \cos \pi\nu \times \int_0^t d\tau (t - \tau) \cos(\nu V_{12}\tau) \left(\frac{\pi T}{\sinh \pi T \tau} \right)^{2\nu}. \quad (\text{S49})$$

The last expression is valid for $\nu < 1/2$, it should be analytically continued in order to obtain the answer for $\nu \geq 1/2$. For $|V_{12}| \gg T$ one obtains

$$\begin{aligned} 2 \cos \pi\nu \int_0^t d\tau (t - \tau) \cos(\nu V_{12}\tau) \left(\frac{\pi T}{\sinh \pi T \tau} \right)^{2\nu} \\ = 2 \cos \pi\nu \int_0^t d\tau (t - \tau) \cos(\nu V_{12}\tau) \tau^{-2\nu} \\ = \frac{\pi(\nu|V_{12}|)^{2\nu-1}}{\Gamma(2\nu)} t \times \left(1 + O\left([\nu|V_{12}|t]^{-\min(2\nu,1)}\right) \right), \end{aligned} \quad (\text{S50})$$

which leads to Eq. (S45). As an analytic function, this answer is valid for any $\nu > 0$, including $\nu = 1$. For $\nu = 1$ our results reproduce those of Ref. [7], with $v^{-\nu}$ playing the role of the density of states of a lead.

It is interesting to note that the dephasing rate (S45), and more generally (S49), does not depend on the value of η_{ref} . It is a consequence of the fact that each quasiparticle that passes through the box causes a state-dependent phase rotation of the box state, and those that tunnel through the reference arm do not. Dephasing is generated by the inability to track the number of quasiparticles that have passed through the box. In the case of $\eta_{\text{ref}} = 0$, one is not able to distinguish different box states by measuring I_{T12} , as can be seen from Eqs. (9,10) of the main text. Yet we note that dephasing does take place, albeit one can restore coherence between different box states by counting the number of quasiparticles transferred between the leads. For $\eta_{\text{ref}} \neq 0$ one cannot restore phase coherence by simply counting the number of quasiparticles as each transferred quasiparticle could have traveled either through the box or through the reference arm. The relation of the dephasing to the number of quasiparticles transferred through the box results in the same voltage dependence of the dephasing rate (S45) and the current I_{T12} (10).

Having in mind possible experimental realizations, we estimate the typical decay time of the off-diagonal matrix element for $\nu = 1/3$ to be ≈ 10 ns when $\eta_{\text{ref}} \approx \eta_{\text{cot}}$ and $I_{T12} \approx 10$ pA, which is a realistic value of tunneling current. Under these conditions, the measurement time

is limited by the time required to accumulate sufficient statistics in order to distinguish the values of I_{T12} for different r .

IV. THE ALGEBRA OF OPERATORS ACTING IN THE 2-BOX DEGENERATE SUBSPACE AND THEIR EIGENSTATES

The 2-box degenerate subspace is spanned by states $|Q_1 \bmod 2\rangle$ that are eigenstates of operator $e^{i\pi\hat{Q}_1}$. All the operators of the form $\hat{\alpha}_{j_2,s}\hat{\alpha}_{j_1,s}^\dagger$ acting in this subspace can be expressed through $e^{i\pi\hat{Q}_1}$ and $e^{i\pi\hat{S}_2}$. It is of importance, therefore, to study the properties of these two operators.

It follows from Eq. (S12) that

$$[\hat{Q}_1, e^{i\pi\hat{S}_2}] = \nu e^{i\pi\hat{S}_2}. \quad (\text{S51})$$

Using this fact and the arbitrariness of choosing the phases of the basis states $|Q_1 \bmod 2\rangle$, one can define

$$|Q_1 \bmod 2\rangle = e^{i\pi\nu^{-1}(Q_1 \bmod 2)\hat{S}_2} |Q_1 \bmod 2 = 0\rangle, \quad (\text{S52})$$

$$e^{i\pi\hat{S}_2} |Q_1 \bmod 2\rangle = |Q_1 + \nu \bmod 2\rangle. \quad (\text{S53})$$

The eigenstates $|S_2 \bmod 2\rangle$ of $e^{i\pi\hat{S}_2}$ have the form

$$\begin{aligned} |S_2 \bmod 2\rangle = \frac{1}{\sqrt{n}} \sum_{r=0}^{n-1} e^{-i\pi r(S_2 \bmod 2)} \\ \times |Q_1 \bmod 2 = \nu r\rangle \end{aligned} \quad (\text{S54})$$

with $n = 2/\nu$. Conversely, the $|Q_1 \bmod 2\rangle$ states can be expressed through $|S_2 \bmod 2\rangle$ via relation (11) in the main text.

V. N-BOX STATE MANIPULATION WITH QADS

Here we elaborate on how transferring a quasiparticle between two QADs each of which is connected to one parafermion allows one to manipulate the state of an N -box. Such a manipulation involves two QADs, each described by Hamiltonian (12). Due to coupling to the parafermions, a fractional quasiparticle can hop between the QADs through the box, which is described by the effective cotunneling Hamiltonian $H_{\text{cot,QAD}}$. Consider the initial state of the QADs being $|1\rangle_1|0\rangle_2$, i.e., QAD1 is filled and QAD2 is empty. The box states can be expanded in $|r, \{X\}\rangle$, the eigenbasis of $\hat{\alpha}_{j_2,s}\hat{\alpha}_{j_1,s}^\dagger$ (S43), where $\hat{\alpha}_{j_1,s}$ and $\hat{\alpha}_{j_2,s}$ are the parafermions to which QAD1 and QAD2 are coupled respectively.

The cotunneling Hamiltonian transforms

$$|1\rangle_1|0\rangle_2|r, \{X\}\rangle \rightleftharpoons |0\rangle_1|1\rangle_2|r, \{X\}\rangle. \quad (\text{S55})$$

Therefore, the problem splits into a set of 2×2 problems each described by

$$H_r = \begin{pmatrix} \Delta V/n & \eta_{\text{cot}}^* e^{-i\nu(\pi r + \delta\varphi/2)} \\ \eta_{\text{cot}} e^{i\nu(\pi r + \delta\varphi/2)} & -\Delta V/n \end{pmatrix}, \quad (\text{S56})$$

where $\Delta V = V_{\text{QAD1}} - V_{\text{QAD2}}$.

Consider the Landau-Zener problem $\Delta V = \lambda t/\nu$ for this Hamiltonian. Then the initial state $|\psi(t_i \rightarrow -\infty)\rangle = |1\rangle_1 |0\rangle_2 |r, \{X\}\rangle$ at large times becomes

$$|\psi(t \rightarrow +\infty)\rangle = e^{i\varphi_0(t)} \left[e^{-\pi\gamma - i\varphi_0(t)} |1\rangle_1 |0\rangle_2 |r, \{X\}\rangle + \frac{\sqrt{2\pi\gamma}}{\Gamma(1+i\gamma)} e^{-\frac{1}{2}\pi\gamma + i\varphi_0(t)} \frac{\eta_{\text{cot}}}{|\eta_{\text{cot}}|} e^{i\nu(\pi r + \delta\varphi/2)} |0\rangle_1 |1\rangle_2 |r, \{X\}\rangle \right], \quad (\text{S57})$$

where $\gamma = |\eta_{\text{cot}}|^2/\lambda$, and

$$\varphi_0(t) = \frac{\lambda t^2}{4} + \frac{1}{2}\gamma \ln(\lambda t^2) - \frac{3\pi}{8}. \quad (\text{S58})$$

In particular, the probability of not transferring a quasiparticle between the QADs is

$$P_{\text{LZ}} = \exp(-2\pi\gamma). \quad (\text{S59})$$

Therefore, by changing the QAD voltages slowly ($\lambda \rightarrow 0$, $\gamma \rightarrow +\infty$), one can transfer the quasiparticle with probability 1; the system final state will then be

$$e^{i\nu(\pi r + \delta\varphi/2)} |0\rangle_1 |1\rangle_2 |r, \{X\}\rangle = |0\rangle_1 |1\rangle_2 \hat{\alpha}_{j_2,s}^\dagger \hat{\alpha}_{j_1,s}^\dagger |r, \{X\}\rangle, \quad (\text{S60})$$

up to an r -independent overall phase. Moreover, if one performs the operation with non-vanishing speed λ and measures the QADs' state in the end one will find the system in one of the states

$$|1\rangle_1 |0\rangle_2 |r, \{X\}\rangle \text{ or } |0\rangle_1 |1\rangle_2 \hat{\alpha}_{j_2,s}^\dagger \hat{\alpha}_{j_1,s}^\dagger |r, \{X\}\rangle \quad (\text{S61})$$

up to r -independent overall phases with probabilities P_{LZ} and $1 - P_{\text{LZ}}$ respectively. One can repeat the operation until the transfer of a quasiparticle has happened. One way or the other, transferring a quasiparticle between the dots implements the action of the $\hat{\alpha}_{j_2,s}^\dagger \hat{\alpha}_{j_1,s}^\dagger$ operator on the N -box low-energy Hilbert space.

VI. THE APPLICABILITY OF OUR RESULTS TO $\nu = 2/3$ PARA-FERMIONS

The results stated in the main text are applicable, with minor corrections, also to parafermions implemented through $\nu = 2/3$ FQH edges. Here we discuss this issue in some detail. A scheme to implement parafermions in a system involving a pair of spin-unpolarized $\nu = 2/3$ FQH puddles has been proposed in Ref. [8]. The setup there is similar to the setup for obtaining parafermions

at $\nu = 1/(2k+1)$: it involves two FQH edges that are gapped in different regions by either electron tunneling or SC pairing between the edges. The domain walls between these regions give rise to parafermionic operators.

The $\nu = 2/3$ edge has a more complicated structure than a $\nu = 1/(2k+1)$ edge. Namely, it has a charged mode $\hat{\phi}_c$ that is described similarly to the only mode present for $\nu = 1/(2k+1)$ and also a neutral mode $\hat{\phi}_n$ [9, 10] (see, however, Refs. [11, 12]). In the scheme of Ref. [8], the neutral mode is uniformly gapped in the whole system and at low energies only the charged mode is of importance. Therefore, the parafermion operators are low energy projections of the elementary excitation $e^{i\sqrt{\nu}\hat{\phi}_c}$ that carries the electric charge νe and does not excite the neutral mode. Thus, PFs for $\nu = 2/3$ can be described with the same formalism as for $\nu = 1/(2k+1)$.

QADs in $\nu = 2/3$ can host both purely charged $2e/3$ excitations and excitations that have $e/3$ -charge and also excite the neutral mode. Since the latter ones cannot travel through the system of parafermions (the neutral mode is gapped), our results regarding the QAD manipulation of parafermions are directly applicable to the case of $\nu = 2/3$.

The results for measuring the state of parafermions with leads are also applicable, up to a minor modification. The measurement scheme we propose involves not just cotunneling through the PF box but also direct tunneling between the leads (involving the reference arm), in which both the purely charged excitations and those having a neutral component participate. Therefore, the expression for the tunneling current in Eq. (10) of the main text should be modified by replacing $|\hat{\eta}_{\text{T12}}|^2 \rightarrow |\hat{\eta}_{\text{T12}}|^2 + |\eta_n|^2$, where $|\eta_n|^2$ characterizes the strength of tunneling of all the neutral-carrying excitations. Thus, for a given voltage V_{12} , the current I_{T12} gets offset by a constant current, still enabling one to distinguish different states of parafermions. The results for dephasing of the box's reduced density matrix (S44), (S45), are applicable without changes, which is easy to understand: neutral-carrying excitations cannot pass through the system of parafermions and therefore do not contribute to dephasing.

-
- [1] N.H. Lindner, E. Berg, G. Refael, and A. Stern, Phys. Rev. X **2**, 041002 (2012).
 - [2] D.J. Clarke, J. Alicea, and K. Shtengel, Nature Commun. **4**, 1348 (2013).
 - [3] D.J. Clarke, J. Alicea, and K. Shtengel, Nature Phys. **10**, 877 (2014).
 - [4] M. Barkeshli, Phys. Rev. Lett. **117**, 096803 (2016).
 - [5] Y. Kim, D.J. Clarke, and R.M. Lutchyn, arXiv:1703.00498.
 - [6] S. Ganeshan and M. Levin, Phys. Rev. B **93**, 075118 (2016).

- [7] S. Plugge, A. Rasmussen, R. Egger, and K. Flensberg, New J. Phys. **19**, 012001 (2017).
- [8] R.S.K. Mong *et al.*, Phys. Rev. X **4**, 011036 (2014).
- [9] C.L. Kane, M.P.A. Fisher, and J. Polchinski, Phys. Rev. Lett. **72**, 4129 (1994).
- [10] C.L. Kane and M.P.A. Fisher, Phys. Rev. B **51**, 13449 (1995).
- [11] J. Wang, Y. Meir, and Y. Gefen, Phys. Rev. Lett. **111**, 246803 (2013).
- [12] I.V. Protopopov, Y. Gefen, A.D. Mirlin, arXiv:1703.02746.